Regular Article

Particle transport in graphene nanoribbon driven by ultrashort pulses

Doniyor Babajanov[1], Davron U. Matrasulov[1], and Reinhold Egger[2,a]

[1] Turin Polytechnic University in Tashkent, 17. Niyazov Str., 100095 Tashkent, Uzbekistan
[2] Institut für Theoretische Physik, Heinrich-Heine-Universität, 40225 Düsseldorf, Germany

Abstract. We study charge transport in a graphene zigzag nanoribbon driven by an external time-periodic kicking potential. Using the exact solution of the time-dependent Dirac equation with a delta-kick potential acting in each period, we study the time evolution of the population transfer probability and the time-dependent optical conductivity. By variation of the kicking parameters, the conductivity becomes widely tunable.

1 Introduction

Ever since its experimental discovery a decade ago, the physics of graphene has been a hot topic in condensed matter physics (see Refs. [1–7] for reviews). One of the most intensely studied class of problems concerns electronic transport in bulk or confined graphene monolayers. We here focus on the particle dynamics in externally driven graphene samples, where a general goal is to achieve tunability of charge transport. A rich variety of predicted and observed phenomena due to time-dependent fields have been reported in recent publications [8–15].

In particular, reference [8] argues that time-periodic spin-orbit interactions lead to an interesting time evolution of the spin polarization and of the optical conductivity. Particle transport can also be induced by a time-dependent elastic deformation field [9], or in a.c. driven graphene nanoribbons, where by adopting a tight-binding model, the authors of reference [13] found a strong dependence of transport properties on the geometry of the ribbon edges. Furthermore, Ishikawa [14] studied electron transport in graphene perturbed by a time-periodic vector potential, which results in an enhancement of interband transitions. Finally, electron transport and current resonances in the presence of a time-dependent scalar potential barrier have been studied in reference [15], where a resonant enhancement of both electron backscattering and the currents across and along the barrier was reported when the modulation frequencies satisfy certain resonance conditions.

Ultrafast dynamics and particle transport in graphene driven by ultrashort optical pulses have also been studied recently [16–22]. The experimental observation of a bright broadband photoluminescence in graphene interacting with femtosecond laser pulses was reported in reference [18]. Moreover, the authors of reference [22] have studied the modification of the bandstructure under ultrashort optical pulses and the carrier dynamics caused by the optical response of graphene, arguing that the electron dynamics in the time-dependent electric field of the laser pulse becomes irreversible, with a large residual conduction band population. In addition, the formation of a laser-induced band gap was discussed in reference [20].

In this paper, we study electron transport in graphene nanoribbons interacting with an external time-periodic scalar potential represented by a sequence of δ-kicks. The setup is schematically shown in Figure 1. Such a potential could be created by applying laser pulses to free-standing samples. Using the exact solution of the time-dependent Dirac equation within one kicking period, we compute the transport properties of the system, such as the probability current and the optical conductivity, as a function of time. As we have discussed above, periodically driven graphene could be realized through the interaction with a.c. voltages [13], pulsed laser fields [23], surface acoustic waves [24], or time-periodic straining [9]. Here we focus on the case of ultrashort optical pulses [16–19].

Let us mention at this stage that some time ago, both the classical and the quantum dynamics of systems interacting with a delta-kicking potential have been extensively studied in the context of nonlinear dynamics and quantum chaos theory [25–27]. A remarkable feature of periodically driven quantum systems is the quantum localization phenomenon, which implies a suppression of the growth of the average kinetic energy with time; for the corresponding classical system, this energy grows linearly in time. However, the case of delta-kicked graphene nanoribbons
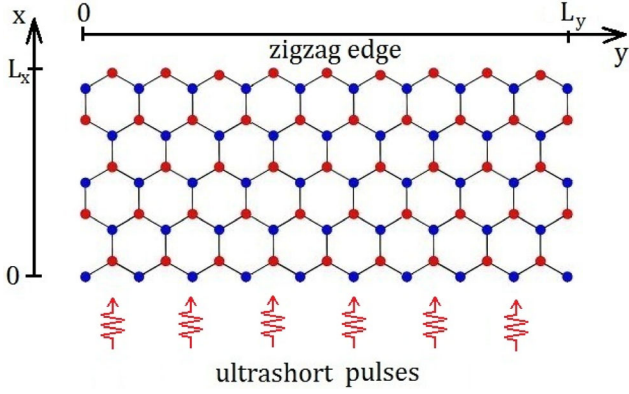
a e-mail: egger@thphy.uni-duesseldorf.de

Fig. 1. Sketch of a kicked zig-zag graphene nanoribbon of width L_x and length L_y. Ultrashort periodic pulses applied to the nanoribbon act as kicking potential.

is more complicated due to the kicking-field-induced population transfer discussed below, which is also the reason for interesting electronic and transport phenomena. The main effect of the driving force is to cause inter- and intra-band transitions, leading to excitation and "ionization" of valence-band electrons to the conduction band. Another effect caused by driving fields in graphene is an effective band-gap opening or widening [20], which allows one to tune the electronic properties using an external time-dependent field. Below, we analyze the time evolution of the population transfer probability and the optical conductivity in delta-kicked graphene nanoribbons. We find that the population transfer probability effectively describes intra- or inter-band anticrossings, where the time-dependent effective density of states reaches a local maximum when anticrossings take place. This effect may increase the number of charge carriers in the conduction band, with a subsequent increase of the current and of the optical conductivity. Indeed, as shown by our analysis of the time-dependent conductivity in Section 3, depending on the kicking parameters, the conductivity may monotonically grow in time, while in other kicking regimes, such a growth is suppressed.

The remainder of this paper is organized as follows. In Section 2 we briefly recall the Dirac equation for graphene zigzag nanoribbons, basically following the approach of Brey and Fertig [28], and discuss the solution of the time-dependent Dirac equation in the presence of the δ-kicking potential. This solution is then utilized to compute the time evolution of the population transfer probability, and, in Section 3, the optical conductivity in different kicking regimes. Finally, Section 4 contains some concluding remarks. Below we often use units where $\hbar = 1$.

2 Kicked graphene nanoribbon

2.1 Unperturbed Hamiltonian

In this work we study the electronic behavior of kicked zigzag graphene nanoribbons, see Figure 1 for an

illustration, within the Dirac equation approach [28]. It is well-established that low-energy quasiparticles in an extended graphene sheet are accurately described by the massless two-dimensional (2D) Dirac Hamiltonian [1]

$$H_0 = v_F \begin{pmatrix} 0 & p_x - ip_y \\ p_x + ip_y & 0 \end{pmatrix}, \qquad (1)$$

where $p_{x,y} = -i\partial_{x,y}$, and $v_F \approx 10^6$ m/sec denotes the Fermi velocity. The 2×2 matrix structure of H_0 is with respect to sublattice space, corresponding to the (A/B-type) basis atoms of graphene's honeycomb lattice [1]. Since we do not take into account electron-electron interaction effects here, the two different valleys (K points) as well as the two spin projections decouple, and we can focus on a single-valley spinless system in equation (1). The spinor eigenstates of the zigzag nanoribbon with periodic boundary conditions along the longitudinal y-direction (see Fig. 1), are written as:

$$\psi(x,y) = \frac{e^{ik_y y}}{\sqrt{L_y}} \Phi(x), \quad \Phi(x) = \begin{pmatrix} \phi_A(x) \\ \phi_B(x) \end{pmatrix}, \qquad (2)$$

where k_y is the conserved wave number along the y-direction. Periodic boundary conditions yield $k_y = 2\pi n_y/L_y$ with integer n_y. To take into account the zigzag edges at $x = 0$ and $x = L_x$, where L_x is the width of the nanoribbon, we impose the boundary conditions [28]

$$\phi_A(L_x) = \phi_B(0) = 0, \qquad (3)$$

and put $0 \le x \le L_x$ henceforth.

Next we summarize the spinor solutions $\psi_n(x,y)$ solving the stationary Dirac equation for eigenenergy E_n in the absence of the kicking potential,

$$H_0 \psi_n(x,y) = E_n \psi_n(x,y), \quad n = (n_x, n_y), \qquad (4)$$

where the integer n_x serves as a band index and n_y parametrizes k_y. The boundary conditions (3) imply that the eigenvalues of equation (4) are obtained from the transcendental equation [28]

$$\frac{k_y - z}{k_y + z} = e^{-2L_x z}, \qquad (5)$$

which admits two type of solutions, namely (i) confined modes (standing waves), and (ii) surface states.

We start by discussing solutions of type (i), which are purely imaginary, $z_{n_x} = ik_x$, and lead to the eigenenergies

$$E_n = \pm v_F \sqrt{k_x^2 + k_y^2}, \qquad (6)$$

where the upper (lower) sign corresponds to the conduction (valence) band. Equation (5) now simplifies to:

$$k_y = \frac{k_x}{\tan(k_x L_x)}, \qquad (7)$$

and solutions for k_x (labeled by $n_x = 1, 2, \ldots$) correspond to confined modes. The respective eigenstate (2), with
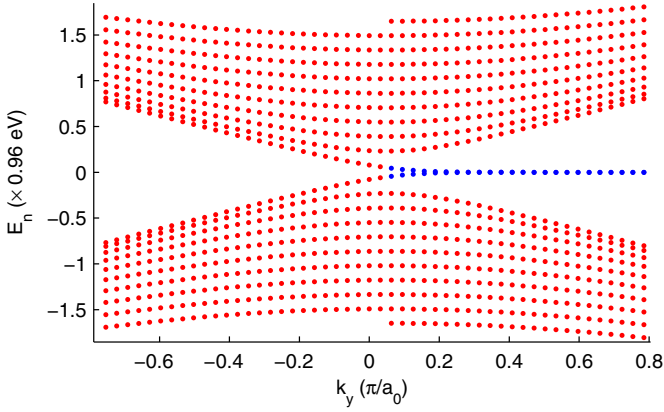
Fig. 2. Band structure of unperturbed graphene nanoribbon. The red dots indicate eigenenergies of confined modes, and the blue dots correspond to surface states. The nanoribbon has width $L_x = 4.92$ nm and length $L_y = 12.3$ nm, and $a_0 = 0.246$ nm is the lattice unit.

the energy E_n in equation (6), has the transverse wave-function

$$\Phi_n(x) = \mathcal{N}_n \left(\begin{array}{c} \sin(k_x x) \\ \pm \frac{i v_F}{E_n}[-k_x \cos(k_x x) + k_y \sin(k_x x)] \end{array} \right), \quad (8)$$

with normalization constant $\mathcal{N}_n$.

Next we turn to surface state (type (ii)) solutions. These correspond to purely real $z = k_x$ in equation (5), where the eigenstate reads:

$$\Phi_n(x) = \mathcal{N}'_n \left(\begin{array}{c} 2 \sinh(k_x x) \\ \frac{v_F}{E_n}[k_y \sinh(k_x x) - k_x \cosh(k_x x)] \end{array} \right). \quad (9)$$

The eigenenergy is now given by:

$$E_n = \pm v_F \sqrt{k_y^2 - k_x^2}, \quad (10)$$

and $\mathcal{N}'_n$ is another normalization constant. The surface state energies equal zero for sufficiently large positive k_y, but they are absent for $k_y < 0$. In Figure 2, the resulting bandstructure of a typical graphene zigzag nanoribbon is plotted.

2.2 Including the kicking potential

We are now ready to include the external driving potential. We consider a periodic sequence of delta-kicks of kicking strength ε and period T. (No confusion with the symbol for temperature should arise here; we always consider the zero-temperature limit.) Writing $H = H_0 + V \mathrm{diag}(1,1)$, the additional term is given by the time-periodic scalar potential,

$$V(x,t) = \varepsilon \cos (2\pi x/\lambda) \sum_{l=0}^{\infty} \delta(t - lT), \quad (11)$$

where λ is the wavelength of the kicking pulse. Experimentally, such delta-kicks could be realized by standing-wave

laser pulses [29–31], or by half-cycle laser pulses [32]. For instance, the delta-kicked quantum rotor, representing a well-known paradigm of quantum chaos theory, can be experimentally realized in ultracold atoms that interact with the periodic standing wave of a near-resonant laser field [29]. Significant progress concerning the experimental realization of graphene interacting with ultrashort laser pulses has also been reported recently [17–19]. Combining the experimental methods in references [29–32] with those in references [17–19] could allow to implement the delta-kicked graphene nanoribbon discussed here in the lab.

The dynamics of a state $\Psi = \Psi(x, y, t)$ is then governed by the time-dependent 2D Dirac equation, $i\partial_t \Psi = H\Psi$. To solve this equation, we expand $\Psi(x, y, t)$ in terms of the complete set of eigenfunctions of the unperturbed graphene zigzag nanoribbon discussed in Section 2.1,

$$\Psi(x, y, t) = \sum_n A_n(t)\psi_n(x, y), \quad (12)$$

where $n = (n_x, n_y)$ and the summation implicitly includes the $\pm$ sign for the conduction and valence band, respectively. To ensure normalization, the initial values (at time $t = 0$) of the complex-valued expansion coefficients $A_n(t)$ in equation (12) satisfy the condition

$$\sum_n |A_n(0)|^2 = 1. \quad (13)$$

Within one time period, the amplitude A_n then follows the time evolution

$$A_n(t + T) = \sum_{n'} V_{nn'} e^{-iE_{n'}T} A_{n'}(t) \quad (14)$$

where E_n is the unperturbed eigenenergy of the respective mode (see Sect. 2.1), and we define the matrix elements

$$V_{nn'} = \int_0^{L_x} dx \int_0^{L_y} dy \; \psi_{n'}^\dagger(x,y) e^{i\varepsilon \cos(2\pi x/\lambda)} \psi_n(x,y), \quad (15)$$

where nonzero matrix elements exist only for $n_y = n'_y$ due to the translation invariance in y-direction. In calculating these matrix elements, we use a well-known Bessel function expansion formula for the exponential term.

In numerical calculations, one may choose only a few non-zero initial coefficients $A_n(0)$ subject to equation (13). In particular, we tested the impact of using different choices for $A_n(0)$, such as randomly chosen or equally distributed values. All choices were found to give qualitatively similar results for the time-evolved state $\Psi(t)$ after many kicks. For the calculations presented below, we chose a random distribution for the coefficients $A_n(0)$ containing ≈15 non-zero entries, where we take into account only states with energy E_n below the Fermi level. The Fermi level is here assumed at the neutrality point, i.e., $E_F = 0$, in order to maximally emphasize the Dirac fermion nature of the graphene nanoribbon. Our procedure for choosing the initial values for the A_n coefficients mimics the zero-temperature average over the filled Fermi sea. We have
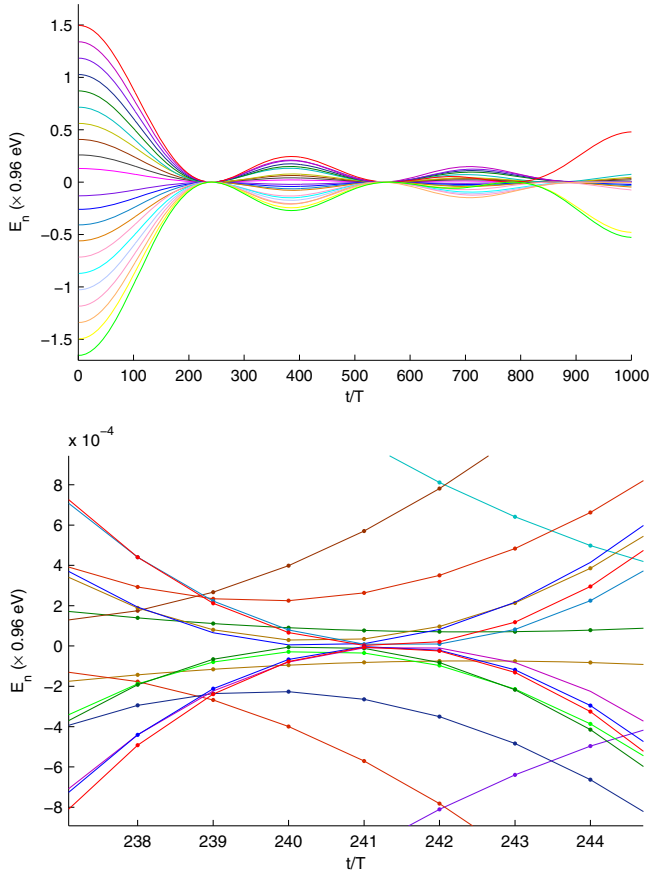
Fig. 3. The upper panel shows the time evolution of the population transfer probability, $\tilde{E}_n(t)$, for a few selected bare energy levels. The lower panel shows the same but on a magnified scale near the first (anti-)crossing. The ribbon width L_x and length L_y were chosen as in Figure 2. The kicking strength is $\varepsilon = 2.7 \times 10^{-13}$ eVs, with period $T = 0.1$ fs and wavelength $\lambda = 2.46$ nm.

carefully checked that different initial values lead to the same physical results after a short initial transient.

Given the wave function, one can compute different characteristics of the carrier dynamics and, in particular, investigate charge transport in a kicked graphene nanoribbon. In Figure 3, the time evolution of the population transfer probability $\tilde{E}_n(t) \equiv |A_n(t)|^2 E_n$ (see Ref. [33]), is shown for a few selected states. We observe several crossings of the quantities $\tilde{E}_n(t)$ within the conduction (or within the valence) band. However, the $\tilde{E}_n(t)$ originating from different bands exhibit an anticrossing, closely approaching each other up to some time when they start to separate again. After a certain number of kicks, one can then again observe crossings or anticrossings, where intra- and interband transitions become more frequent. Since initially the valence band is filled, this can lead to an increase in the number of electrons in the conduction band, and thereby to current flow. A related enhancement of intra- and inter-band transitions has also been reported in reference [22] for graphene subject to ultrashort laser pulses. When the $\tilde{E}_n(t)$ separate from each other again after a

crossing or anticrossing, intra- and interband transitions become less frequent, and one can expect a decrease in the current. Such features indeed appear in the conductivity, as we study next.

3 Optical conductivity

The interaction of external electromagnetic fields with solids generally causes a modification of their electronic properties and, in particular, of the bandstructure [22,34]. Using the solution of the time-dependent Dirac equation for delta-kicking potential discussed in Section 2, one can compute the related population transfer probabilities in Figure 3. In this section, we focus on the optical conductivity of our system, which represents an important observable of experimental interest and can provide precious insights about the transport mechanisms at play in kicked graphene nanoribbons.

Within linear response theory, the Kubo formula yields for the diagonal elements of the time-dependent conductivity tensor ($\alpha = x, y$) [35]

$$\sigma_{\alpha\alpha}(x, y; t, \omega) = \frac{e^2}{\omega} \int_0^\infty d\tau e^{-i\omega\tau}$$
$$\times \langle [J_\alpha(x, y, t), J_\alpha(x, y, t - \tau)] \rangle, \quad (16)$$

where $[,]$ denotes the commutator and the particle current density along the α-direction is [1]

$$J_\alpha(x, y, t) = v_F \Psi^\dagger(x, y, t) \sigma_\alpha \Psi(x, y, t), \quad (17)$$

with standard Pauli matrices $\sigma_{\alpha=x,y}$ acting in sublattice space. The average in equation (16) is taken with respect to the filled Fermi sea at the initial time $t = 0$, present before the kicking potential is switched on. In equation (16), we focus on the long-wavelength limit by probing the two current operators appearing in the Kubo formula at the same point in space. In terms of the expansion coefficients $A_n(t)$ appearing in the expansion (12), equation (17) takes the form

$$J_\alpha(x, y, t) = v_F \sum_{nn'} A_{n'}^*(t) A_n(t) \psi_{n'}^\dagger(x, y) \sigma_\alpha \psi_n(x, y),$$
$$(18)$$

where A^* denotes the complex conjugate of A. Inserting equation (18) into equation (16), the conductivity at time t follows as a lengthy (but straightforwardly obtained) expression involving the time-dependent coefficients $\{A_n(t')\}$ for $0 < t' < t$. As described in Section 2.2, the zero-temperature average over the filled Fermi sea is implemented by choosing suitable initial values for those coefficients. Below we discuss the time-dependence of the conductivity averaged over the sample area and taken in the $\omega \to 0$ limit,

$$\sigma_{\alpha\alpha}(t) = \lim_{\omega \to 0} \text{Re} \int_0^{L_y} \frac{dy}{L_y} \int_0^{L_x} \frac{dx}{L_x} \sigma_{\alpha\alpha}(x, y; t, \omega). \quad (19)$$

Notice that the respective conductivity (for $\omega \to 0$) in the undriven case simply corresponds to the $t = 0$ limit in
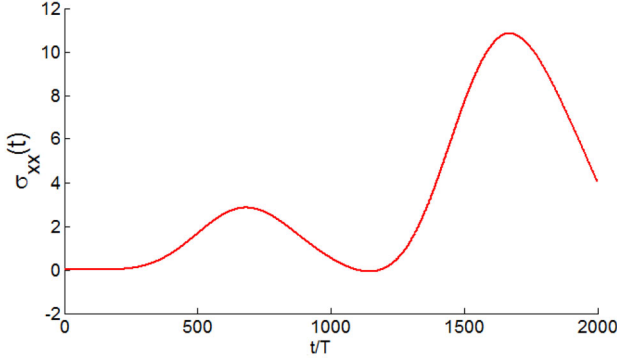
Fig. 4. Conductivity $\sigma_{xx}(t)$ in units of $e^2/\hbar$, see equation (19), as a function of time for a kicked graphene nanoribbon. Parameters are as in Figure 3 but with kicking time period $T = 1$ fs.
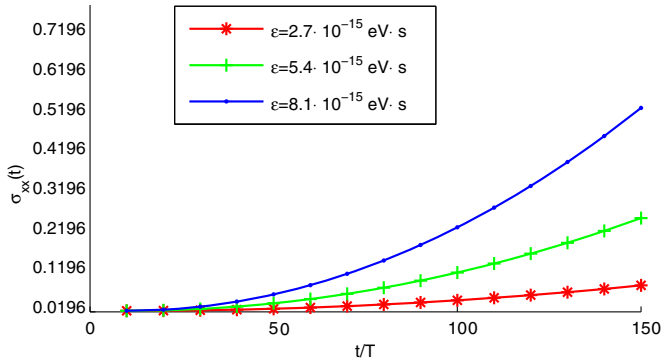

Fig. 5. Same as Figure 4 but for several values of the kicking strength ε, and showing only the initial time period ($t < 150T$).
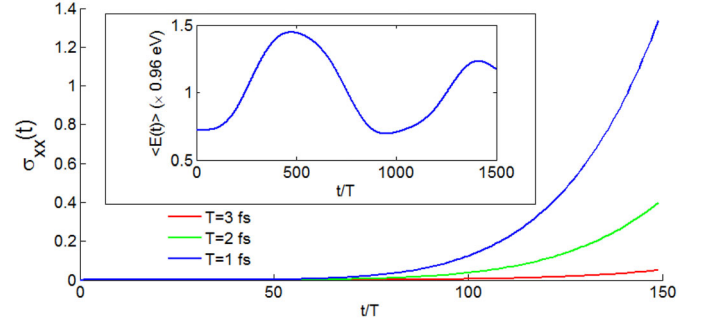

Fig. 6. Same as Figure 5 but for different kicking periods T and the fixed kicking strength $\varepsilon = 2.7 \times 10^{-13}$ eVs. The inset shows the time dependence of the average kinetic energy on a longer time scale for $T = 1$ fs.
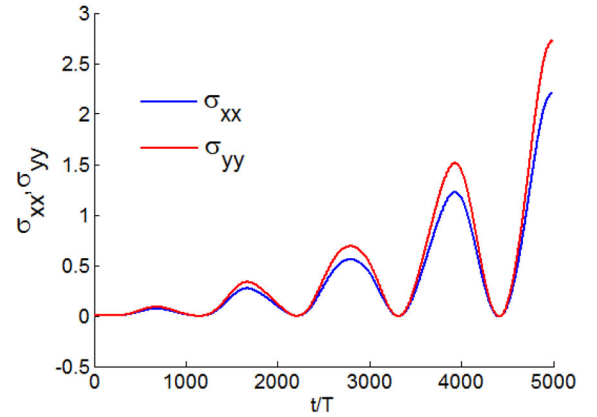

Fig. 7. Time-dependence of the longitudinal conductivities $\sigma_{xx}(t)$ and $\sigma_{yy}(t)$ (in units of $e^2/\hbar$) along the x- and y-direction, respectively, for the parameters in Figure 4.

the figures shown below. Since we take the Fermi energy at zero energy, this $t = 0$ value is generally orders of magnitude smaller than the conductivity at long times in the driven case.

Figure 4 shows numerical results for $\sigma_{xx}(t)$ for representative kicking potential parameters. We observe that $\sigma_{xx}(t)$ grows during some initial time interval, followed by a suppression of the growth along with the development of oscillatory behavior. These features can be linked to the presence of crossings and anticrossings of the population transfer probability as discussed above.

Next, Figure 5 presents $\sigma_{xx}(t)$ for a fixed kicking period, $T = 1$ fs, but now for different values of the kicking strength ε. For the shown regime of rather short times, the conductivity monotonically grows in time. Clearly, for larger kicking strength, $\sigma_{xx}(t)$ grows more rapidly, where the slope of the growth is approximately proportional to ε. However, as seen in Figure 4, after a longer time span, the conductivity will be suppressed again. Nonetheless, the variation of the kicking strength allows for a considerable tunability of the conductivity.

The dependence of the conductivity on a variation of the kicking period T (with fixed strength ε) is illustrated by Figure 6. We find that $\sigma_{xx}(t)$ monotonically grows within the considered time interval, although at larger

times (not shown) the conductivity decreases and becomes quasioscillatory again, as displayed before in Figure 4. The inset of Figure 6 also shows the time-dependence of the average kinetic energy,

$$\langle E(t) \rangle = \int_0^{L_x} dx \int_0^{L_y} dy \, \Psi^*(x,y,t) H_0 \Psi(x,y,t)$$
$$= \sum_n |A_n(t)|^2 E_n. \tag{20}$$

This quantity exhibits time-periodic behavior, again reflecting the periodic appearance of band crossings as illustrated by Figure 3. Such a behavior is different from a localization-induced saturation expected from quantum chaos theory but also differs from the simple monotonic growth expected on classical grounds [25–27].

Next, in Figure 7, we compare the different components of the conductivity, namely $\sigma_{xx}(t)$ and $\sigma_{yy}(t)$. Although the kicking force acts along x-direction, we find very similar values for the conductivities in both directions. The spectral rearrangement caused by the kicking force is thus quite efficient in also inducing current fluctuations in the transverse (y) direction.

Finally, Figure 8 presents the spatio-temporal evolution of the probability density, $|\Psi(x,y,t)|^2$. Since
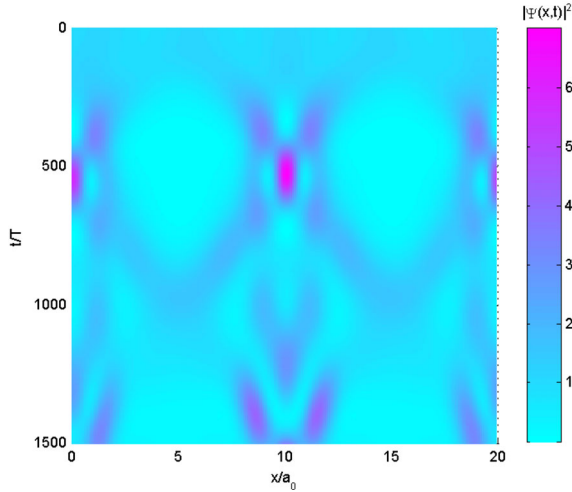
Fig. 8. Probability density as a function of time and coordinate for the parameters in Figure 4 (note that $L_x = 20a_0$).

the result is homogeneous along the y-direction, we show it as 2D color-scale plot in the (x, t) plane; note the symmetry under spatial reflection with respect to the ribbon midpoint $x = L_x/2$. Figure 8 provides additional information about the possibility of spatio-temporal quantum localization of electrons in the kicked graphene nanoribbon. In fact, we conclude from Figure 8 that the carriers are not fully localized inside the ribbon, although signatures of localization near the midpoint are visible for finite time spans. These time spans match up with the conductivity peaks in Figure 4, and suggest that for these parameters, the main transport channels are located away from the midpoint. Note that a significant average velocity increase is apparent in Figure 8 whenever the conductivity increases.

4 Concluding remarks

In this paper, we have studied time-dependent particle transport in graphene zigzag nanoribbons driven by an external time-periodic δ-kicking potential. The time-dependent Dirac equation can be solved exactly within a single kicking period, and numerical iteration of this solution provides access to the wave function at arbitrary time. Using this wave function, we have computed the time-dependent optical conductivity (and other quantities). The conductivity is observed to initially grow as a function of time up to certain time, after which the conductivity decreases and ultimately shows quasioscillatory behavior.

We find it rather remarkable that by judiciously choosing the strength ε and the time period T of the kicking field, one can achieve almost arbitrary results for the oscillation period and for the amplitude of the conductivity. In particular, it is possible to choose parameters such that the initial increase extends for very long time. The described behavior of $\sigma_{\alpha\alpha}(t)$ can be linked to the existence

of (anti-)crossings in the population transfer probabilities of the driven system.

The model studied in our work could be realized in zigzag ribbons made of monolayer graphene samples that are exposed to standing-wave ultrashort laser pulses, such as those discussed in references [29–31]. The above results also may help in solving the problem of tunable charge transport in graphene-based electronic devices.

References

1. A.H. Castro Neto, F. Guinea, N.M.R. Perez, K.S. Novoselov, A.K. Geim, Rev. Mod. Phys. **81**, 109 (2009)
2. N.M.R. Peres, Rev. Mod. Phys. **82**, 2673 (2010)
3. S. Das Sarma, S. Adam, E.H. Hwang, E. Rossi, Rev. Mod. Phys. **83**, 407 (2011)
4. A.V. Rozhkov, G. Giavaras, Y.P. Bliokh, V. Freilikher, F. Nori, Phys. Rep. **503**, 77 (2011)
5. A.H. Castro Neto, K. Novoselov, Rep. Prog. Phys. **74**, 082501 (2011)
6. V.N. Kotov, B. Uchoa, V.M. Pereira, F. Guinea, A.H. Castro Neto, Rev. Mod. Phys. **84**, 1067 (2012)
7. J. Güttinger, F. Molitor, C. Stampfer, S. Schnez, A. Jacobsen, S. Dröscher, T. Ihn, K. Ensslin, Rep. Prog. Phys. **75**, 126502 (2012)
8. A. Scholz, A. Lopez, J. Schliemann, Phys. Rev. B **88**, 045118 (2013)
9. A. Vaezi, N. Abedpour, R. Asgari, A. Cortijo, M.A.H. Vozmediano, Phys. Rev. B **88**, 125406 (2013)
10. A. Lopez, Z.Z. Sun, J. Schliemann, Phys. Rev. B **85**, 205428 (2011)
11. K.-H. Ding, Z.-G. Zhu, J. Berakdar, Phys. Rev. B **84**, 115433 (2011)
12. E. Perfetto, G. Stefanucci, M. Cini, Phys. Rev. B **82**, 035446 (2010)
13. C.G. Rocha, L.E.F. Foa Torres, G. Cuniberti, Phys. Rev. B **81**, 115435 (2010)
14. K.L. Ishikawa, Phys. Rev. B **82**, 201402 (2010)
15. S.E. Savelev, W. Häusler, P. Hänggi, Phys. Rev. Lett. **109**, 226602 (2012)
16. T.M.Rusin, W. Zawadzki, Phys. Rev. B **80**, 045416 (2009)
17. C.H. Lui, K.F. Mak, J. Shan, T.F. Heinz, Phys. Rev. Lett. **105**, 127404 (2010)
18. W.-T. Liu, S.W. Wu, P.J. Schuck, M. Salmeron, Y.R. Shen, F. Wang, Phys. Rev. B **82**, 081408 (2010)
19. A. Roberts, D. Cormode, C. Reynolds, T. Newhouse-Illige, B.J. LeRoy, A.S. Sandhu, Appl. Phys. Lett. **99**, 051912 (2011)
20. H.L. Calvo, H.M. Pastawski, S. Roche, L.E.F. Foa Torres, Appl. Phys. Lett. **98**, 232103 (2011)
21. T. Li, L. Luo, M. Hupalo, J. Zhang, M.C. Tringides, J. Schmalian, J. Wang, Phys. Rev. Lett. **108**, 167401 (2012)
22. H.K. Kelardeh, V. Apalkov, M.I. Stockman, `arXiv:1401.5786` (2014)
23. H.K. Avetissian, A.K. Avetissian, G.F. Mkrtchian, Kh.V. Sedrakian, Phys. Rev. B **85**, 115443 (2012)

24. P. Thalmeier, B. Dora, K. Ziegler, Phys. Rev. B **81**, 041409(R) (2010)
25. G. Casati et al., in *Stochastic Behavior in Classical and Quantum Hamiltonian Systems*, Lecture Notes in Physics (Springer, Berlin, 1979), Vol. 93, p. 334
26. R. Sankaranarayanan, V.B. Sheorey, Phys. Lett. A **338**, 288 (2005)
27. G.M. Izrailev, Phys. Rep. **196**, 299 (1990)
28. L. Brey, H.A. Fertig, Phys. Rev. B **73**, 235411 (2006)
29. F.L. Moore, J.C. Robinson, C.F. Bharucha, B. Sundaram, M.G. Raizen, Phys. Rev. Lett. **75**, 4598 (1995)
30. A. Ullah, M.D. Hoogerland, Phys. Rev. B **83**, 046218 (2012)
31. A. Ullah, S.K. Ruddell, J.A. Currivan, M.D. Hoogerland, Eur. Phys. J. D **66**, 315 (2012)
32. A. Matos-Abiague, J. Berakdar, Phys. Rev. B **69**, 155304 (2004)
33. M. Grifoni, P. Hänggi, Phys. Rep. **304**, 229 (1998)
34. N. Tzoar, J.I. Gersten, Phys. Rev. B **12**, 1132 (1975)
35. A. Altland, B.D. Simons, *Condensed Matter Field Theory*, 2nd edn. (Cambridge University Press, Cambridge, 2010)